Source wavelet effects on the inverse scattering series internal-multiple leading-order-attenuation algorithm and its higher-order modification that accommodate issues that arise when treating internal multiples as subevents

H. Liang and A. Weglein, M-OSRP, University of Houston

April 29, 2013

Abstract

The inverse scattering series (ISS) internal-multiple-attenuation method predicts internal multiples directly and without any subsurface information. The ISS leading-order attenuator of first-order internal multiples is the leading-order term in the subseries that contributes to the removal of first-order internal multiples. The basic idea behind the leading-order attenuator is that all the events in the data are treated as subevents and combined nonlinearly (three data sets are involved), and among all the combinations first-order internal multiples can be predicted by the combination that has all subevents correspond to primaries. While the ISS leading-order attenuator has demonstrated its capability for internal-multiple prediction/attenuation, it has strengths and limitations as implied by "leading-order" and "attenuator". On one hand, the ISS internal-multiple leading-order attenuator predicts exact time and approximate amplitude, but it has specific prerequisites such as knowledge of the source wavelet, as well as source and receiver deghosting, and free-surface-multiple removal. The information omitted from any prerequisite is left for the adaptive subtraction technique to clean up. On the other hand, the entire data set, consisting of primaries and internal multiples, is input into the algorithm. When internal multiples in the data themselves act as subevents, the leading-order attenuator produces not only first-order internal multiples, but also higher-order internal multiples and, at times, spurious events, which have been observed in the tests of Fu et al. (2010) and Luo et al. (2011). Weglein et al. (2011) have also noted this and suggested that the resolution of the problem would reside in other terms of the ISS. Ma et al. (2012) and Liang et al. (2012) identified higher-order terms from the ISS that retain the benefits of the leading-order attenuator while addressing the issues due to spurious events. The higher-order terms require the leading-order term as an ingredient. This report specifically examines the effects of source wavelet on the ISS internal-multiple leading-order attenuator and its higher-order modification. By comparing the internal-multiple and spurious-event prediction results with and without source wavelet deconvolution, we show how the source wavelet affects the shape and amplitude fidelity of the prediction of internal multiples and spurious events.

1 The leading-order ISS internal-multiple-attenuation algorithm

The ISS internal-multiple-attenuation algorithm is a subseries of the inverse scattering series. The algorithm starts with the deghosted input data from which the reference wavefield and free-surface multiples have been removed and source wavelet has been deconvolved, $D(k_g, k_s, \omega)$, where k_g and k_s are the horizontal wavenumbers corresponding to receiver and source coordinates x_g and x_s, respectively, and ω is the temporal frequency.

$$D(k_g, k_s, \omega) = (-2iq_s)^{-1} b_1(k_g, k_s, \omega), \tag{1.1}$$

where $b_1(k_g, k_s, \omega)$ corresponds to an uncollapsed FK migration of effective normal incident spike plane-wave data (Weglein et al., 2003; Hsu et al., 2011). The second term in the algorithm is the leading-order attenuator of first-order internal multiples, which predicts the negative of first-order internal multiples and alters all higher-order internal multiples (the order of an internal multiple is defined by the total number of downward reflections). The leading-order attenuator in a 2D earth is given by Araújo et al. (1994) and Weglein et al. (1997)

$$\begin{aligned} b_3(k_g, k_s, q_g + q_s) = \frac{1}{(2\pi)^2} \int_{-\infty}^{\infty} \int_{-\infty}^{\infty} dk_1 e^{iq_1(z_s - z_g)} dk_2 e^{iq_2(z_g - z_s)} \\ \times \int_{-\infty}^{\infty} dz_1 e^{i(q_g + q_1)z_1} b_1(k_g, -k_1, z_1) \\ \times \int_{-\infty}^{z_1 - \epsilon} dz_2 e^{i(-q_1 - q_2)z_2} b_1(k_1, -k_2, z_2) \\ \times \int_{z_2 + \epsilon}^{\infty} dz_3 e^{i(q_2 + q_s)z_3} b_1(k_2, -k_s, z_3), \end{aligned} \tag{1.2}$$

where c_0 is the reference velocity, $q_g = sgn(\omega)\sqrt{(\frac{\omega}{c_0})^2 - k_g^2}$ and $q_s = sgn(\omega)\sqrt{(\frac{\omega}{c_0})^2 - k_s^2}$ are the vertical wavenumbers, ϵ is a small positive parameter chosen to ensure that the relations between pseudo-depths $z_1 > z_2$ and $z_3 > z_2$ are satisfied, and z_g and z_s are source and receiver depths, respectively.

For a 1D earth and a normal incidence, wave equation 1.2 reduces to

$$b_3(k) = b_3^{PPP} = \int_{-\infty}^{\infty} dz_1 e^{ikz_1} b_1(z_1) \int_{-\infty}^{z_1 - \epsilon} dz_2 e^{-ikz_2} b_1(z_2) \int_{z_2 + \epsilon}^{\infty} dz_3 e^{ikz_3} b_1(z_3), \tag{1.3}$$

where the deghosted data, $D(t)$, for an incident spike wave, satisfy $D(\omega) = b_1(2\omega/c_0)$, and where $b_1(z) = \int_{-\infty}^{\infty} e^{-ikz} b_1(k) dk$, and $k = 2\omega/c_0$ is the vertical wavenumber. Here, we introduce a new notation, b_3^{PPP}, in which the superscript ("P" represents primary, and "I" represents internal multiple) indicates specific events in the data that are input into each of the three integrals. The events indicated in this notation are the ones that the algorithm can accommodate in its goal of removing first-order internal multiples. The data with first-order internal multiples attenuated are

$$D(t) + D_3(t), \tag{1.4}$$

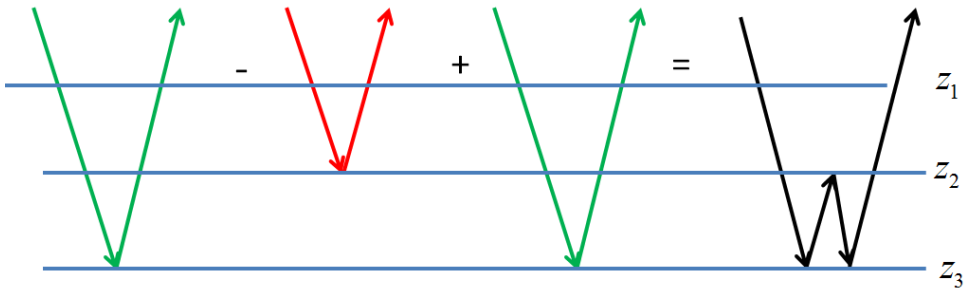

Figure 1: A first-order internal multiple constructed by three primary subevents that satisfy the "lower-higher-lower" pattern in pseudo-depth domain.

where $D_3(t)$ is the inverse Fourier transform of $D_3(\omega)$, and where $D_3(\omega) = b_3(k)$ for an incident spike wave. Weglein and Matson (1998) showed that this algorithm can be interpreted as the subevents construction of internal multiples. Figure 1 illustrates the construction of a first-order internal multiple using three primary subevents. The predicted time of the internal multiple is exact, and the predicted amplitude approximates the true amplitude (Weglein et al., 2003).

2 The higher-order modification of the ISS internal-multiple leading-order-attenuation algorithm

Early analysis of the ISS leading-order attenuator focused on the performance of internal multiples prediction by using subevents that correspond to primaries. However, the input data contain both primaries and internal multiples and all events in the data will be treated as subevents. Under some circumstances treating internal multiples as subevents in the first-order internal-multiple algorithm can lead to spurious events. Ma et al. (2012) and Liang et al. (2012) define the conditions when that can occur and explain how terms further in the ISS address and remove those spurious events. For instance, a spurious event may be generated by the leading-order attenuator when an internal multiple itself is treated as a subevent in the second integral of equation 1.3, as shown in Figure 2. It is worthing noting that in figure 2, the "lower-higher-lower" relationship between the psudeo-depths is required by b_3, and if it not satisfied this kind of subevent combination will not occur in b_3, and such type of a spurious event would not be produced.

Ma et al. (2012) identify a higher-order term from the inverse scattering series that can generate the negative of the spurious event.

$$b_5^{PIP}(k) = \int_{-\infty}^{\infty} dz_1 e^{ikz_1} b_1(z_1) \int_{-\infty}^{z_1-\epsilon} dz_2 e^{-ikz_2} b_3(z_2) \int_{z_2+\epsilon}^{\infty} dz_3 e^{ikz_3} b_1(z_3). \tag{2.1}$$

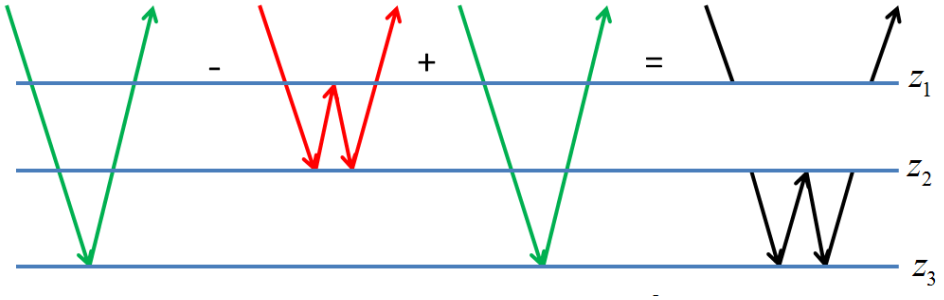

Figure 2: Subevent construction of a spurious event when an internal multiple itself is treated as a subevent in the second integral of the leading-order attenuator (number of reflectors $N >= 3$, and $2z_2 - z_1 < z_3$).

The output of the new ISS internal-multiple algorithm for this three-reflector case is

$$D(t) + D_3(t) + D_5^{PIP}(t), \tag{2.2}$$

where $D_5^{PIP}(t)$ is the inverse Fourier transform of $D_5^{PIP}(\omega)$ and where $D_5^{PIP}(\omega) = b_5^{PIP}(k)$ for spike data. The original algorithm (see equation 1.4) attenuates the first-order internal multiples and preserves primaries but can also output spurious events. The new algorithm in equation 2.2 provides the benefit of the original algorithm while addressing issues that are due to spurious events.

When there are more than three reflectors in the earth, other types of spurious events could also be generated by the leading-order attenuator (Liang et al. (2012)). In this report, we will focus only on the three-reflector case. Therefore, only the leading-order attenuator (equation 1.3) and the higher-order term (equation 2.1) will be examined in this report.

3 The source wavelet effects on ISS internal-multiple prediction exemplified using two examples

In the previous section, the input data are assumed to be source wavelet deconvolved, deghosted, and with free-surface multiples removed. If the data are generated by using a source wavelet instead of an incident spike wave in a 1D case, $b_1(k)$ is obtained by the following equation:

$$D(\omega) = A(\omega)b_1(2\omega/c_0). \tag{3.1}$$

Then, the internal multiples predicted by the leading-order attenuator (equation 1.3), which has opposite polarity as the true internal multiples, are obtained by

$$D_3(\omega) = A(\omega)b_3(\omega/c_0). \tag{3.2}$$

When adding equation 3.2 to equation 3.1, all the first-order internal multiples are attenuated, and higher-order internal multiples are altered. More details on incorporating source wavelet deconvolution into the ISS internal multiple attenuation algorithm can be referred to Yang and Weglein (2013). Including source wavelet deconvolution in the higher-order term for removing spurious event require this initial step in the leading-order attenuator. The predicted spurious events (with opposite polarity as the actual spurious event generated by the leading-order attenuator) are obtained by

$$D_5^{PIP}(\omega) = A(\omega)b_5^{PIP}(\omega/c_0). \tag{3.3}$$

Equations 3.1, 3.2, and 3.3 can be easily extended to multi-dimensional cases. In this section, we will examine the effects of a source wavelet on the prediction of internal multiples and spurious events. we apply the ISS internal-multiple leading-order attenuator and its higher-order modification with and without inclusion of source wavelet deconvolution for both 1D normal incidence and 1.5D shot gather examples, and then compare the results. In this report, we use the spectral division method to deconvolve the source wavelet from the input data. Other methods (e.g., Wiener filter) could also be used and more details about source wavelet deconvolution can be referred to Tang et al. (2012).

3.1 1D normal incidence example

Here we will examine the source wavelet effect on the leading-order attenuator and its higher-order modification (using the exact source wavelet that are used to generate synthetic data). Figure 3 shows a trace generated by the 1D normal-incidence reflectivity method (Ricker source wavelet with peak frequency 30Hz, and sampling interval in time dt=4ms). The reflectivity method can be used to generate primaries and internal multiples separately. In this figure three primaries are shown in red, and all the internal multiples are shown in blue.

Figure 4 shows the actual internal multiples in the data (top) and the internal multiples predicted by using the ISS leading-order attenuator ($-D_3$) without source wavelet deconvolution (bottom). These two results then are normalized by their respective maximum sample value, and plotted together in Figure 5. From Figures 4 and 5 we can see that the predicted time is exact, but the amplitude and shape of the predicted internal multiples are not matched with those of actual internal multiples. From Figure 5 we can also see the spurious event, at time $1.33s$ (in green circle), that is generated by the ISS leading-order attenuator. This event does not exist in the original input data and that's why it is called a spurious event. Figure 6 shows the comparison of the spurious event generated by the leading-order attenuator and the spurious event predicted by the higher-order term (equation 2.1). Both results are obtained without source wavelet deconvolution, and we can see that again the predicted amplitude and shape do not matched with the real ones.

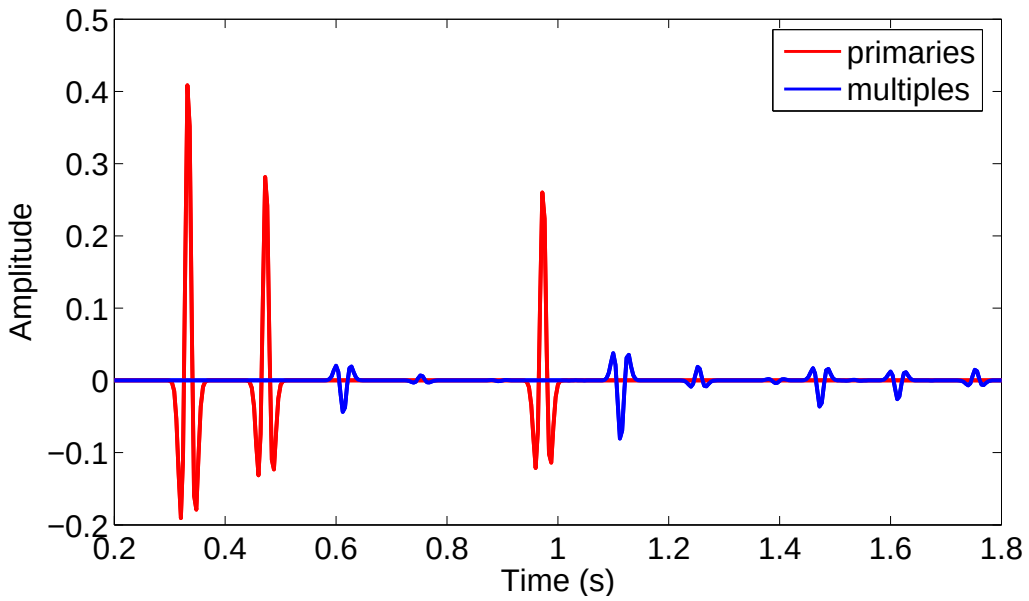

Figure 3: An input trace, including three primaries (red) and all internal multiples (blue).

Next we apply the procedures described in equations 3.1, 3.2, and 3.3 to incorporate the source wavelet deconvolution into internal multiple and spurious event predictions. Figure 7 shows the true internal multiples in the data (red) and internal multiples predicted by the ISS leading-order attenuator ($-D_3$) with source wavelet deconvolution (blue). It is shown that with the source wavelet deconvolution the shape of the internal multiple prediction matches the actual internal multiples very well. Also, the predicted time is exact and the predicted amplitude is approximate.

Figure 8 shows the comparison of the spurious events in D_3 and the spurious event predicted by the higher-order modification($-D_5^{PIP}$), and both results are obtained with source wavelet deconvolution. From the figure we can see that the predicted spurious event matches the one generated by the leading-order attenuator very well. By adding D_5^{PIP} to D_3 the spurious event is greatly attenuated and the internal multiple prediction is almost unchanged (compared to Figure 7), as shown in Figure 9. From Figure 9 we can conclude that the modified internal-multiple-prediction algorithm in equation 2.2 provides the benefit of original algorithm (equation 1.4) while addressing the limitation due to spurious events.

3.2 1.5D shot-gather example

In this section, we examine the source wavelet effects on the ISS internal-multiple leading-order attenuator and its higher-order modification for a 1.5D shot-gather example. The data are generated by using finite-difference code within the M-OSRP group (code courtesy of Fang Liu and Di Chang, and the source wavelet is a Ricker wavelet with 25Hz peak frequency). Figure 10 shows the three-

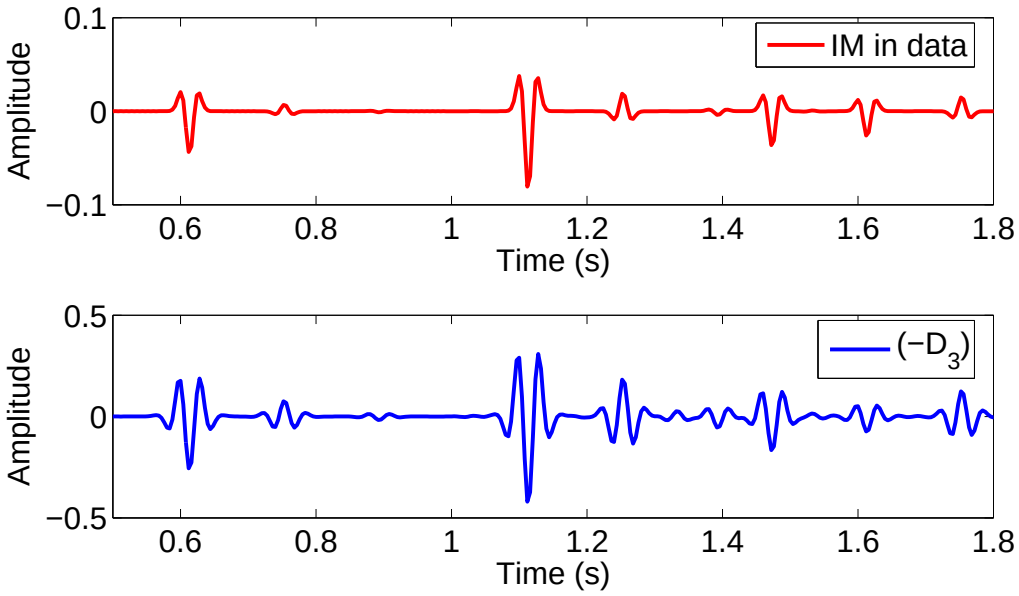

Figure 4: Top: actual internal multiples in the data; bottom: predicted multiples ($-D_3$) without source wavelet deconvolution.

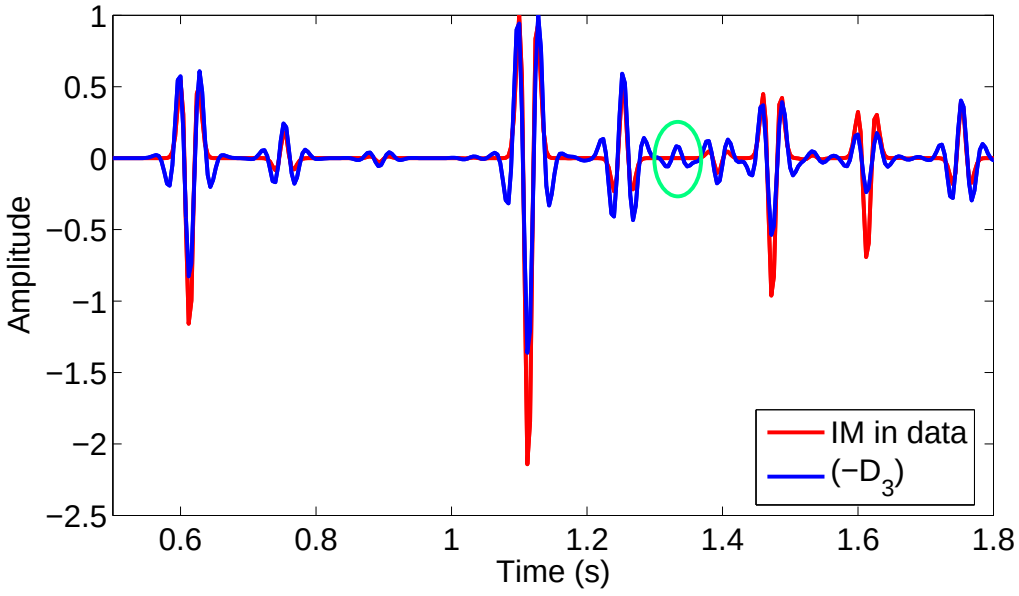

Figure 5: Internal multiples in the data (red) and predicted multiples ($-D_3$) without source wavelet deconvolution (blue). Both results are normalized by their maximum sample value, respectively. The green circle shows the spurious event.

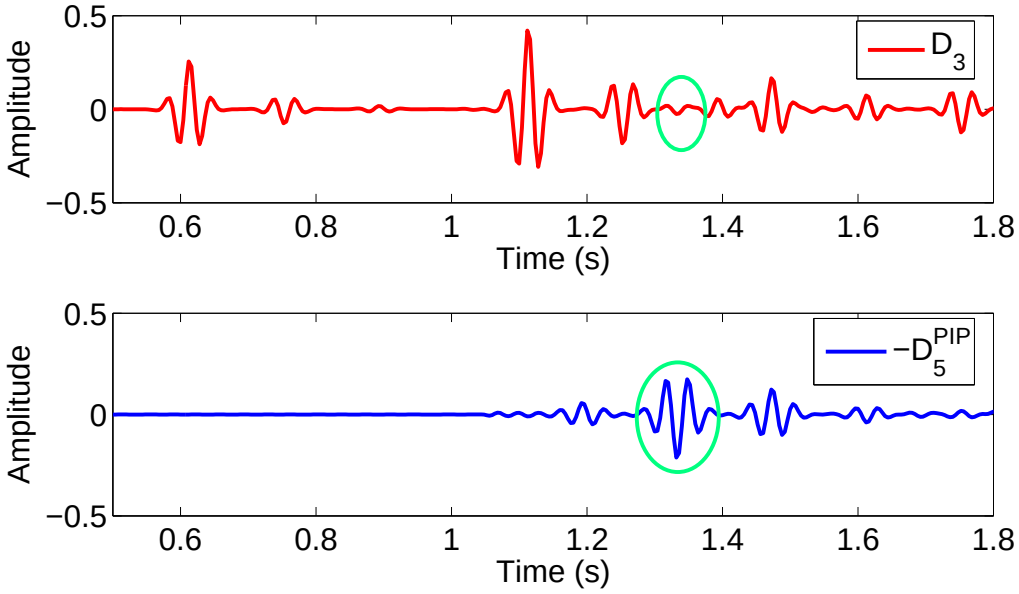

Figure 6: Top is the result of D_3 (spurious event at time 1.33s) and bottom is the result of $-D_5^{PIP}$ (predicted spurious event at time 1.33s). Both results are obtained without source wavelet deconvolution. Green circles show the spurious events.

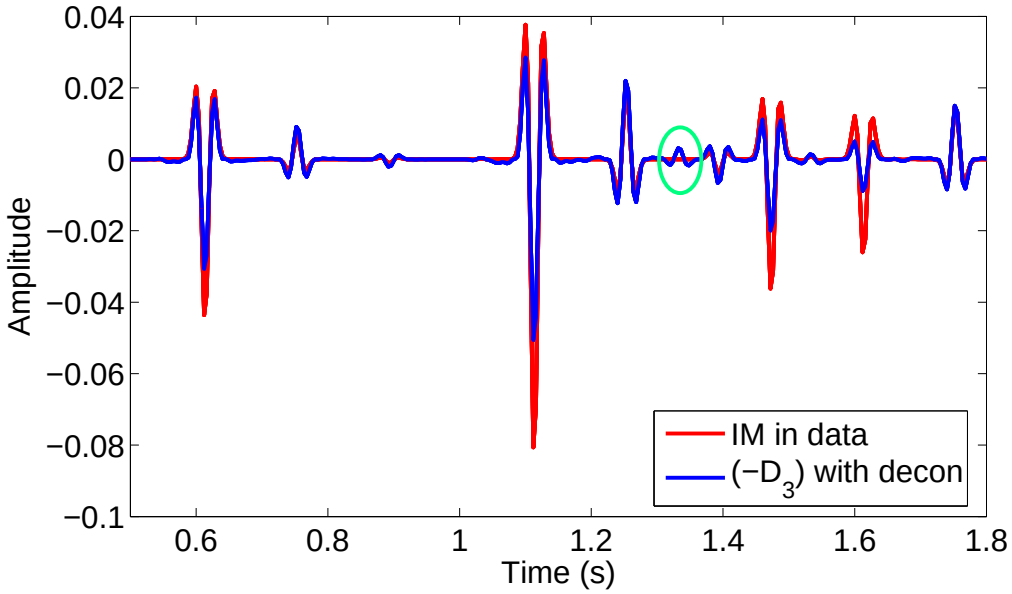

Figure 7: Actual internal multiples in the data (red) and internal multiples predicted by the ISS leading-order attenuator with source wavelet deconvolution (blue).

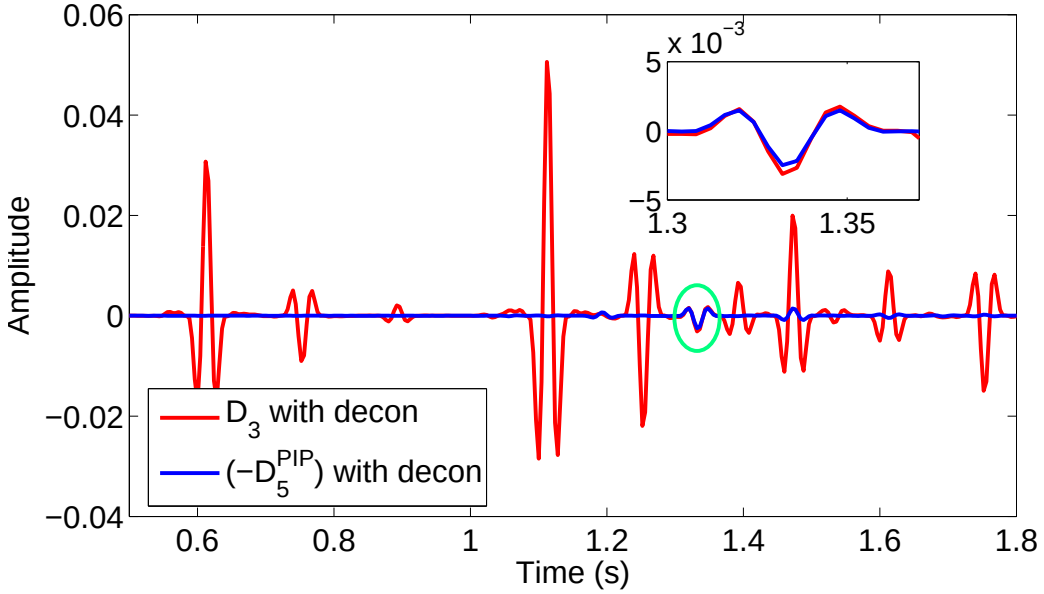

Figure 8: Comparison of spurious events (in green circle) in D_3 and spurious event prediction represented by $-D_5^{PIP}$, and the upper right box shows the zoomed part in the circle; both results are obtained with source wavelet deconvolution.

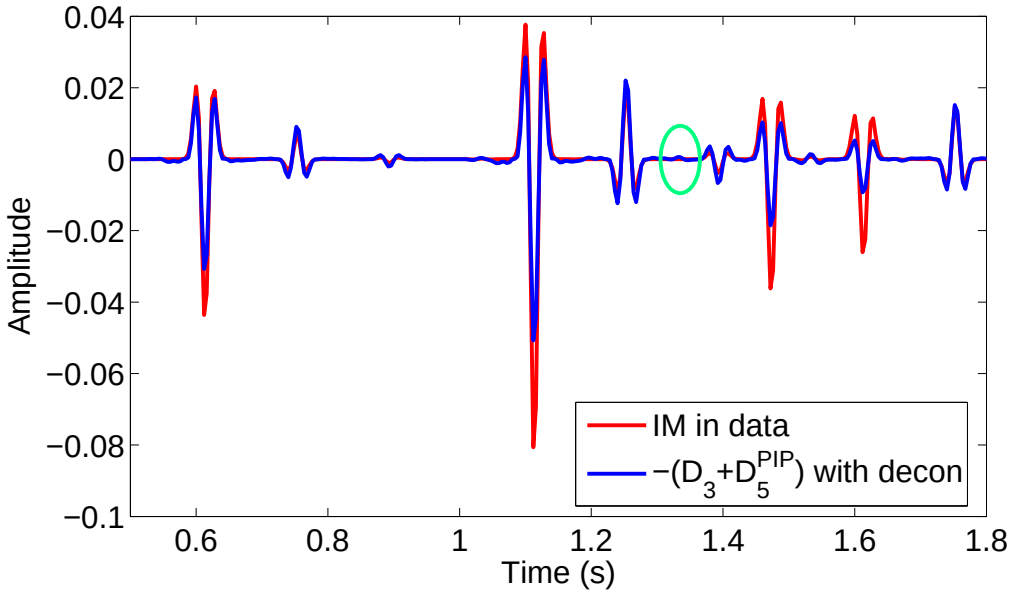

Figure 9: Comparison of actual internal multiples in data (red) and modified prediction represented by $-(D_3 + D_5^{PIP})$ (with source wavelet deconvolution). Green circles correspond to the spurious events.

reflector 1D model for data generation. Figures 11a and 11b show the shot gather without and with source wavelet deconvolution, respectively. The first five events in Figure 11a are: the first primary, the second primary, the first-order and second-order internal multiples generated between the first and second reflectors, and the third primary.

We first examine the source wavelet effects on the leading-order attenuator (b_3 term). Figures 12a and 12b show the predicted multiple ($-D_3$) with (right) and without (left) source wavelet deconvolution. We can see that without source wavelet deconvolution the predicted multiples spread out, and also the amplitudes of the predicted multiples in the two results are very different. Figure 13 shows for comparison wiggle plots of the multiple prediction without deconvolution (13a), the input shot gather (13b), and the multiple prediction with deconvolution (13c). We choose the time window so that all the events shown in the wiggle plots are internal multiples. The results show that with the source wavelet deconvolution, the shapes of the predicted internal multiples are more similar to those of actual internal multiples in the data. Then we compare the amplitudes of the actual internal multiples with those of the multiples predicted using two different schemes, respectively. Figure 14a shows the amplitude comparison of the zero-offset traces from the input shot gather (red) and the multiple predicted without source wavelet deconvolution (blue), and Figure 14b shows the amplitude comparison of zero-offset traces from the input shot gather (red) and the multiple predicted with source wavelet deconvolution (blue). In each of these two figures, the red event at about $1.25s$ is the third primary and the rest of the events are internal multiples. From these two figures we can see that by including the source wavelet deconvolution, the amplitudes of the predicted internal multiples approximate those of the actual internal multiples.

Next we will examine the source wavelet effects on the higher-order term addressing issues due to spurious events, i.e., the b_5^{PIP} term. Figures 15a and 15b show the results of $-D_3$ and D_5^{PIP} without source wavelet deconvolution, and Figures 16a and 16b show the corresponding results with source wavelet deconvolution. We extract the zero traces from each set of two figures and then compare them in the same plot. Figure 17a shows the comparison of zero-offset traces from $-D_3$ and D_5^{PIP}, both of which are obtained without source wavelet deconvolution. Figure 17b shows the comparison of zero-offset traces from $-D_3$ and D_5^{PIP} obtained with source wavelet deconvolution. From the results in these two figures, we can see that with the source wavelet deconvolution, both the amplitude and shape of the predicted spurious event match well those of actual spurious event generated by the leading-order attenuator.

3.3 Internal multiple prediction using estimated wavelet

In this section we estimated the source wavelet using the Green's theorem-derived method (Weglein and Secrest (1990)) and then use this estimated source wavelet to repeat the process in the Section 3.2. Further details about the source wavelet estimation based on Green's theorem and its application can be referred to Mayhan et al. (2012). It is worth noting that in this report the actual medium is an inhomogeneous acoustic medium with water on the top and the reference medium is a whole-water medium. Therefore, the total wavefield in the actual medium contains direct wave,

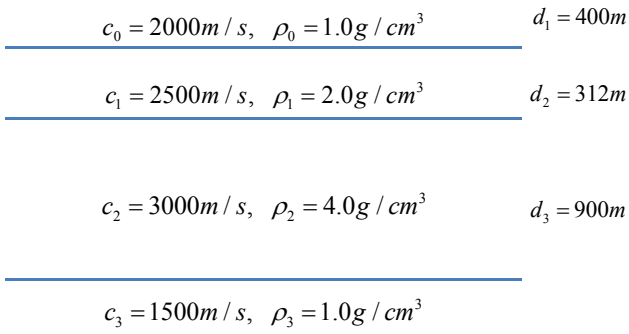

Figure 10: 1D model with both velocity and density variations.

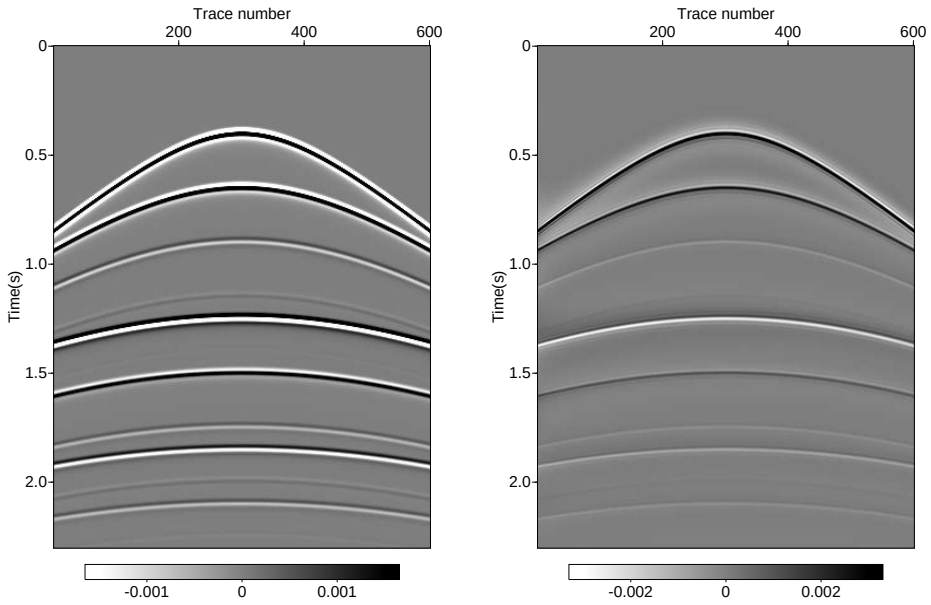

(a) (b)

Figure 11: (a) Shot gather without source wavelet deconvolution; (b) shot gather with source wavelet deconvolution.

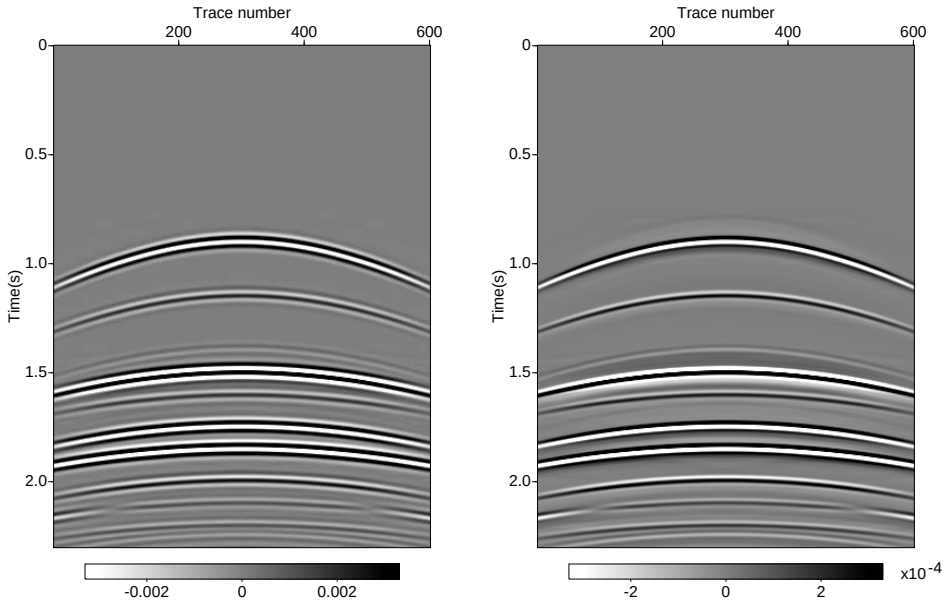

(a) (b)

Figure 12: Internal-multiple prediction ($-D_3$) without (a) and with (b) source wavelet deconvolution.

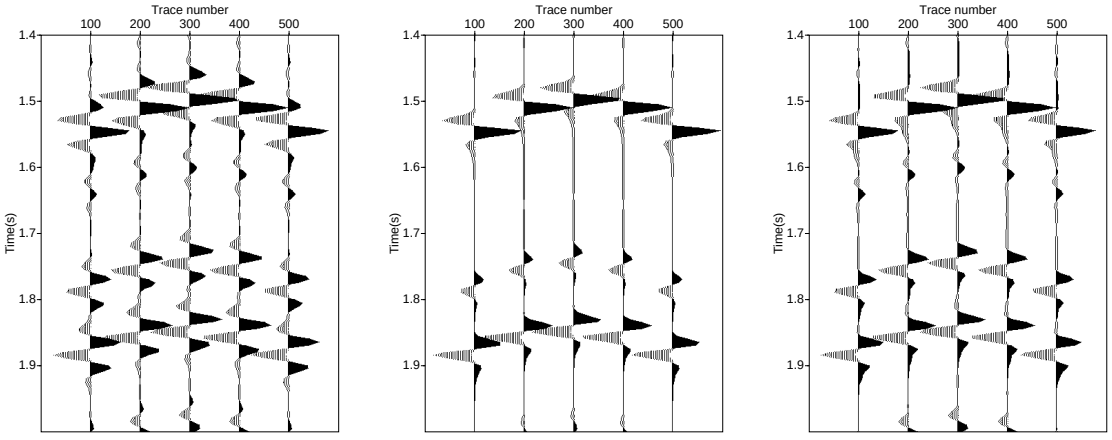

(a) (b) (c)

Figure 13: Wiggle plots of selected traces: (a) a multiple prediction without source wavelet deconvolution, (b) an input shot gather, (c) and a multiple prediction with deconvolution.

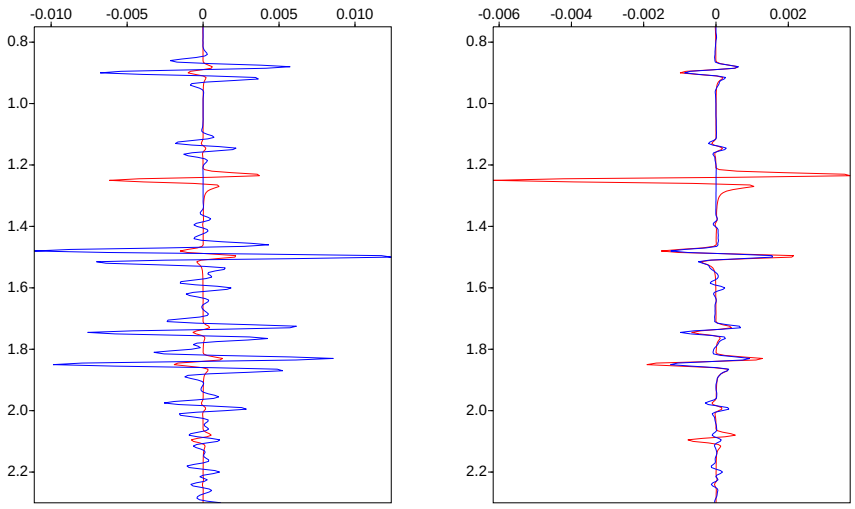

(a) (b)

Figure 14: (a) Comparison of the zero-offset traces extracted from Figures 11a (red) and 12a (blue); (b) Comparison of the zero-offset traces extracted from Figures 11a (red) and 12b (blue).

primaries and internal multiples while the reference wavefield in the reference medium contains direct wave only. The key equation of the source wavelet estimation is as follows,

$$\tilde{A}(\omega)G_0(\mathbf{r},\mathbf{r}_s,\omega) = \oint_S [\tilde{P}(\mathbf{r}',\mathbf{r}_s,\omega)\nabla' G_0(\mathbf{r}',\mathbf{r},\omega) - G_0(\mathbf{r}',\mathbf{r},\omega)\nabla'\tilde{P}(\mathbf{r}',\mathbf{r_s},\omega)]\cdot\mathbf{n}dS, \tag{3.4}$$

where $\mathbf{r_s}$, $\mathbf{r}'$, $\mathbf{r}$ represent the locations of source, receiver and prediction points, respectively; $\tilde{P}(\mathbf{r}',\mathbf{r}_s,\omega)$ is the Fourier transform of the pressure field, $G_0(\mathbf{r_i},\mathbf{r_j},\omega)$ is the Fourier transform of the Green's function in the reference medium. The source wavelet $A(\omega)$ can be obtained by averaging the reference wavefield divided by a Green's function:

$$A(\omega) = \frac{1}{N}\sum_{i=1}^{N}\frac{\tilde{P}_0(\mathbf{r}_i,\mathbf{r}_s,\omega)}{G_0(\mathbf{r}_i,\mathbf{r}_s,\omega)}. \tag{3.5}$$

From the equation 3.4 we can see that both the total wavefield and its derivative are needed to estimate the source wavefield. We calculate the derivative of the wavefield using the measured wavefield at two different depths:

$$\frac{dP}{dz} = \frac{P(205m) - P(200m)}{5m}. \tag{3.6}$$

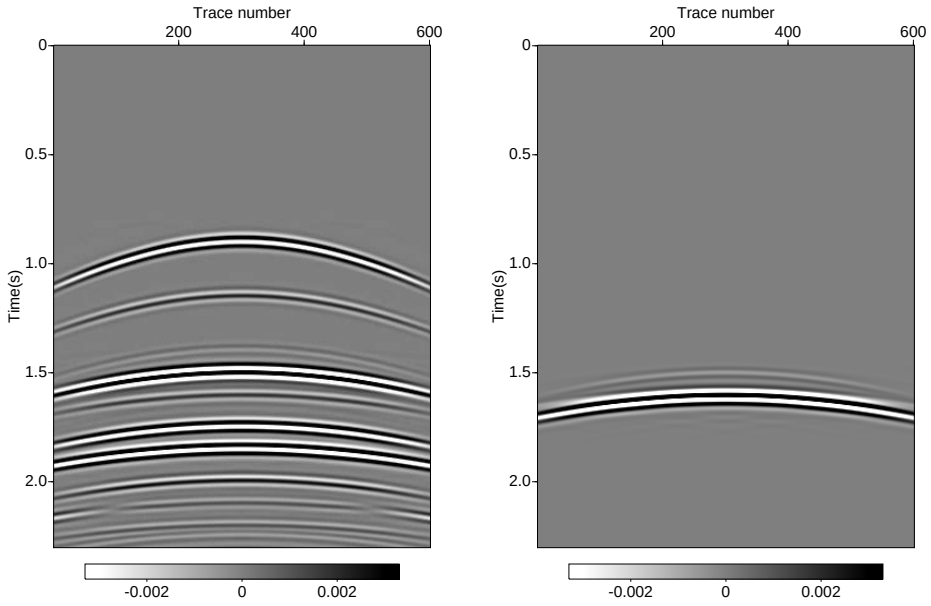

(a) (b)

Figure 15: Results without source wavelet deconvolution: (a) multiple prediction ($-D_3$) and (b) spurious-event prediction (D_5^{PIP}).

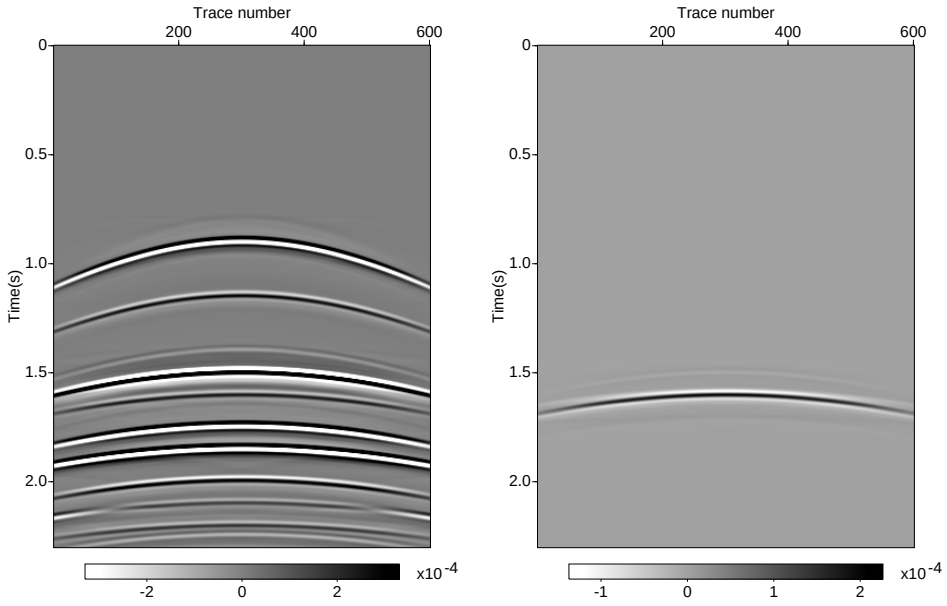

(a) (b)

Figure 16: Results with source wavelet deconvolution: (a) multiple prediction (- D_3) and (b) spurious event prediction (D_5^{PIP}).

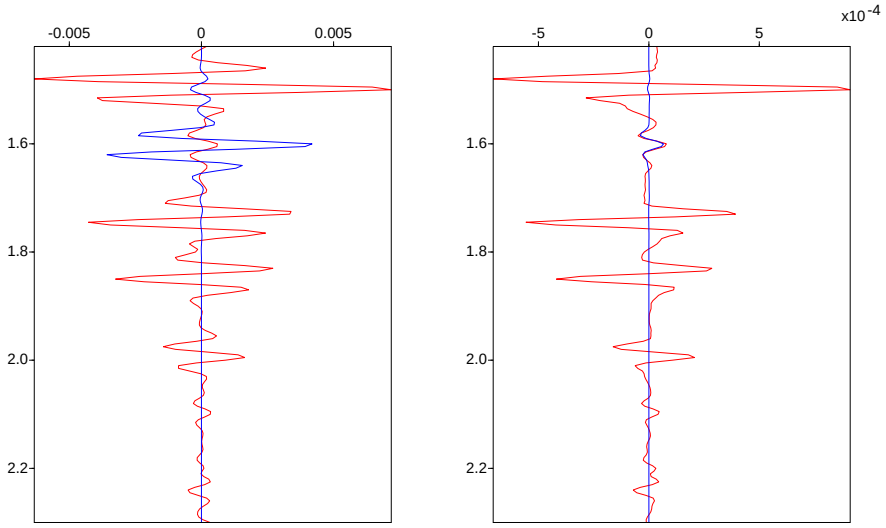

(a) (b)

Figure 17: (a) Comparison of the zero-offset traces extracted from Figures 15a (red) and 15b (blue); (b) Comparison of the zero-offset traces extracted from Figures 16a (red) and 16b (blue).

Figure 18a shows that the estimated source wavelet (blue) matches well the actual source wavelet (red). Figure 18b shows zero-offset traces of predicted internal multiples using actual (red) and estimated source wavelet (blue), and Figure 18c shows zero-offset traces of predicted spurious event using actual (red) and estimated source wavelet (blue). We can see that the results by using the estimated waevlets matches the resutls by using the actual wavelet.

4 Summary and discussion

We examine the source wavelet effects on both the ISS internal-multiple leading-order attenuator and higher-order term for removing spurious event by comparing the internal-multiple-prediction results with and without source wavelet deconvolution. From the comparison we can see that by including the source wavelet deconvolution in the ISS internal-multiple prediction, both the shape and amplitude of the predicted internal multiples can be improved (made closer to the true internal multiples). The accuracy of the source wavelet is important for the test results, and we have shown that the source wavelet can be estimated using Green's theorem.

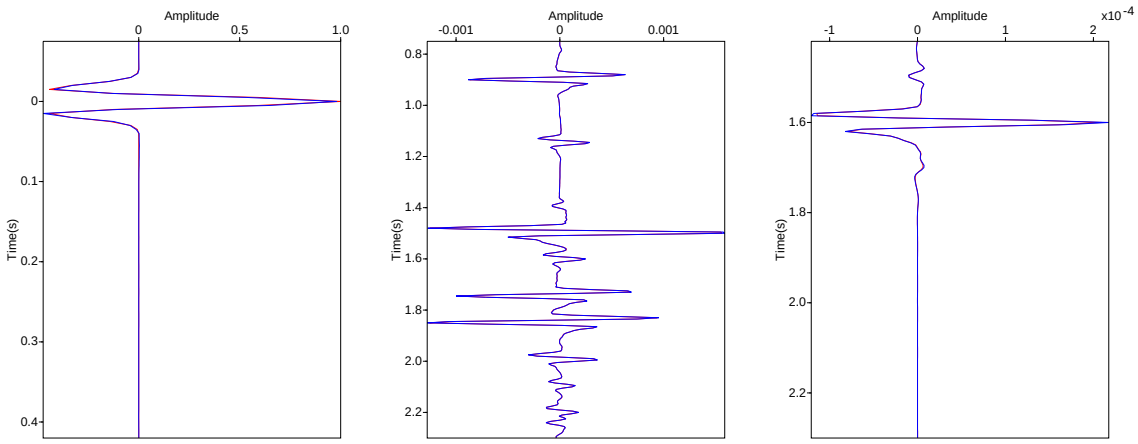

(a) (b) (c)

Figure 18: (a) Comparison of actual (red) and estimated (blue) source wavelets; (b) zero-offset traces of predicted internal multiples using actual (red) and estimated source wavelet (blue) (c) zero-offset traces of predicted spurious events using actual (red) and estimated source wavelet (blue).

5 Acknowledgements

The first author would like to thank Schlumberger/Westerngeco for the internship during Fall 2012 and for the permission to present the work. We are also grateful to all M-OSRP sponsors for their support of this research. Special thanks to Wilberth Herrera and Chao Ma for reviewing this report, and Jim Mayhan and Lin Tang for their help.

References

Araújo, F. V., A. B. Weglein, P. M. Carvalho, and R. H. Stolt. "Inverse scattering series for multiple attenuation: An example with surface and internal multiples." SEG Technical Program Expanded Abstracts (1994): 1039–1041.

Fu, Q., Y. Luo, G. K. Panos, S. Huo, G. Sindi, S. Hsu, and A. B. Weglein. "The inverse scattering series approach towards the elimination of land internal multiples." SEG Technical Program Expanded Abstracts (2010): 3456–3461.

Hsu, S., P. Terenghi, and A. B. Weglein. "The properties of the inverse scattering series internal multiple attenuation algorithm: Analysis and evaluation on synthetic data with lateral variations, choosing reference velocity and examining its sensitivity to near surface properties." Mission-Oriented Seismic Research Program (M-OSRP), Annual Report (2011): 16–28.

Liang, H., C. Ma, and A. B. Weglein. "A further general modification of the leading order ISS attenuator of first order internal multiples to accommodate primaries and internal multiples when an arbitrary number of reflectors generate the data: theory, development, and examples." M-OSRP 2011 Annual meeting (2012).

Luo, Y., P. G. Kelamis, Q. Fu, S. Huo, G. Sindi, S. Hsu, and A. B. Weglein. "Elimination of land internal multiples based on the inverse scattering series." The Leading Edge (2011): 884–889.

Ma, C., H. Liang, and A. B. Weglein. "Modifying the leading order ISS attenuator of first-order internal multiples to accommodate primaries and internal multiples: fundamental concept and theory, development, and examples exemplified when three reflectors generate the data." M-OSRP 2011 Annual meeting (2012).

Mayhan, J., A. B. Weglein, and P. Terenghi. "Green's theorem-derived preprocessing of marine seismic data." Mission-Oriented Seismic Research Program (M-OSRP), Annual Report (2012): 9–113.

Tang, L., P. Terenghi, and A. B. Weglein. "Application of the Wiener filter in wavelet estimation using Kristin data." Mission-Oriented Seismic Research Program (M-OSRP), Annual Report (2012): 267–276.

Weglein, A. B., F. V. Araújo, P. M. Carvalho, R. H. Stolt, K. H. Matson, R. T. Coates, D. Corrigan, D. J. Foster, S. A. Shaw, and H. Zhang. "Inverse Scattering Series and Seismic Exploration." Inverse Problems (2003): R27–R83.

Weglein, A. B., F. A. Gasparotto, P. M. Carvalho, and R. H. Stolt. "An inverse-scattering series method for attenuating multiples in seismic reflection data." Geophysics (1997): 1975–1989.

Weglein, A. B., S. Hsu, P. Terenghi, X. Li, and R. Stolt. "Multiple attenuation: Recent advances and the road ahead 2011." The Leading Edge (2011): 864–875.

Weglein, A. B. and K. H. Matson. "Inverse scattering internal multiple attenuation: an analytic example and subevent interpretation." Mathematical Methods in Geophysical Imaging V (1998): 108–117.

Weglein, A. B. and B. G. Secrest. "Wavelet estimation for a multidimensional acoustic or elastic earth." Geophysics (1990): 902–913.

Yang, J. and A. B. Weglein. "ISS internal multiple attenuation algorithm with source wavelet." Mission-Oriented Seismic Research Program (M-OSRP), Annual Report (2013).